Archives of Acoustics Vol. 48, No. 3, pp. 373–380 (2023), doi: 10.24425/aoa.2023.145242

Research Paper

Design and Experiments of a New Internal Cone Type Traveling Wave Ultrasonic Motor

Ye CHEN(1)*, Junlin YANG(1), Liang LI(2), Shihao XIAO(1)

(1) *Institute of Vibration Engineering, Liaoning University of Technology*
Shiying Street, Guta District, Jinzhou, Liaoning Province, China

(2) *College of Science, Liaoning University of Technology*
Shiying Street, Guta District, Jinzhou, Liaoning Province, China

*Corresponding Author e-mail: jxchenye@lnut.edu.cn

(*received November 25, 2022; accepted March 12, 2023*)

In order to simplify the motor structure, to reduce the difficulty of rotor pre-pressure application and to obtain better output performance, a new internal cone type rotating traveling wave ultrasonic motor is proposed. The parametric model of the internal cone type ultrasonic motor was established by the ANSYS finite element software. The ultrasonic motor consists of an internal cone type vibrator and a tapered rotor. The dynamic analysis of the motor vibrator is carried out, and two in-plane third-order bending modes with the same frequency and orthogonality are selected as the working modes. The other advantages of this motor are that pre-pressure can be imposed by the weight of the rotor. The prototype was trial-manufactured and experimentally tested for its vibration characteristics and output performance. When the excitation frequency is 22260.0 Hz, the pre-pressure is 0.1 N and the peak-to-peak excitation voltage is 300 V, the maximum output torque of the prototype is 1.06 N · mm, and the maximum no-load speed can reach 441.2 rpm. The optimal pre-pressure force under different loads is studied, and the influence of the pre-pressure force on the mechanical properties of the ultrasonic motor is analyzed. It is instructive in the practical application of this ultrasonic motor.

Keywords: ultrasonic motors; traveling wave; internal cone type; bending vibration.

1. Introduction

The ultrasonic motor is a new type of micro-technical motor that uses the inverse piezoelectric effect of piezoelectric materials to produce ultrasonic frequency vibration in the vibrator and uses the friction between the vibrator and the rotor to achieve the rotor rotation, linear or multi-degree-of-freedom motion. Ultrasonic motors have the advantages of a simple structure, high power density, fast response, no electromagnetic radiation, and high positioning accuracy (Zhao, 2011). Therefore, more and more scholars have explored and researched them from the aspects of structure design, drive control principle and friction materials, and have achieved certain results (Tian *et al.*, 2020; Makarem *et al.*, 2021; Li *et al.*, 2019; Puoza, Sakthivelsamy, 2021; Wang *et al.*, 2020). Now ultrasonic motors have been successfully applied in precision positioning systems, micro-robotic systems, aerospace engineering, biological engineering and other high-tech industrial settings (Liu *et al.*, 2022; Olsson *et al.*, 2016; Mishra *et al.*, 2018; Wang, Xu, 2017; Oh *et al.*, 2009).

Ultrasonic motors can be divided into standing wave ultrasonic motors and traveling wave ultrasonic motors from the point of view of vibration characteristics. In commercial applications, the latter are widely used because of their high efficiency and simpler drive control. From the viewpoint of a motion output, they can be divided into rotary, linear and multi-degree-of-freedom ultrasonic motors (Ryndzionek, Sienkiewicz, 2021). Among them, rotary ultrasonic motors are more well developed and the technology is more mature. Among various types of ultrasonic motors, squiggle and in-plane bending travelling wave ultrasonic motors are often suitable for miniaturiza-

tion and integration (Xu *et al.*, 2021; Lu *et al.*, 2020; Mashimo, Oba, 2022; Li *et al.*, 2021).

An important factor affecting the application of the ultrasonic motor is the overall structural size. Therefore a millimeter scale thick film rotating traveling wave ultrasonic motor based on the chemical mechanical thinning and polishing process is proposed (Zhang *et al.* 2022). The vibration mode of the motor is the B02 mode under the resonant frequency of 26.2 kHz. The motor can achieve stable bidirectional rotation under the excitation of four sinusoidal voltages. Moreover, when the excitation voltage is 50 V_{p-p}, the maximum speed can reach 766 rpm under the preload force of 0.686 mN. A miniature flat cross-shaped rotating ultrasonic motor was designed and manufactured (Čeponis *et al.* 2020). The motor rotates the rotor by exciting the first-order in-plane bending vibration of the cross-shaped vibrator. The results of the experimental study show that the motor has a maximum speed of 972.62 rpm at a peak-to-peak of 200 V when a preload force of 22.65 mN is applied. The miniature cross-shaped motor can be mounted directly to a printed circuit board or integrated into other systems with a limited installation space.

The oblate-type ultrasonic motor, extensively desired in small-scale robotics, fuzing, and biomedical technology, however, has not obtained abundant development. A flat ultrasonic micro-motor with multilayer piezoelectric ceramics and a chamfered driving tip is proposed in order to realize a low-voltage drive for ultrasonic motors (Zhao *et al.* 2016). The vibrator is fabricated with a multilayer piezoelectric ceramic glued to a copper ring with a thickness of 0.5 mm. There are six driving tips on the copper ring as a whole. The driving tips are chamfered in the proper direction and their height is 1 mm. The motor can work smoothly and reach a rotation speed of about 2000 r/min at a voltage amplitude of 20 V_{p-p}. It shows the characteristics of high speed and low load capacity.

As can be seen from the above-mentioned articles, many authors have paid attention to motor miniaturization and structural innovations. Therefore, this paper proposes an internal cone type rotating traveling wave ultrasonic motor, which consists of an internal cone type vibrator and a tapered rotor, and uses friction to drive the rotor in a rotational motion. The internal cone type vibrator and the tapered rotor are in trapezoidal teeth contact with each other, which facilitates the smooth operation of the motor while having a large output speed and an output torque.

2. Ultrasonic motor structure and working principle

2.1. Ultrasonic motor structure

The structure of the internal cone type ultrasonic motor vibrator is shown in Fig. 1. The internal cone

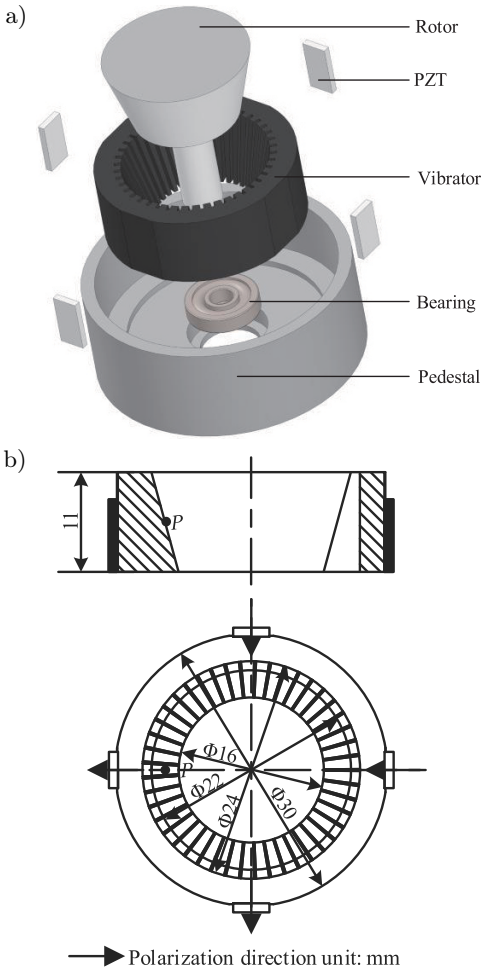

Fig. 1. Structure of ultrasonic motor: a) 3D model of the motor; b) main geometrical parameters of the vibrator.

type vibrator is based on a cylindrical structure with a tapered hole inside. Several uniform inner trapezoidal teeth are designed inside the cylinder, which is conducive to enlarging the amplitude of the inner surface in the circumferential direction. The number of teeth in the vibrator is 45, and the width of the tooth slot is 0.2 mm. Four rectangular piezoelectric ceramic sheets of $8 \times 4 \times 1$ mm are pasted on the outer surface of the internal cone type vibrator. The diameter of the outer cylindrical surface of the internal cone type vibrator of the rotating ultrasonic motor is set to 30 mm.

In Fig. 1, the tapered rotor of the motor and the internal cone type vibrator are in contact with the bevel tooth surface, which is very different from the point contact structure in the contact process between the vibrator and the rotor of the previous motor, which can ensure the stable contact between the vibrator and the rotor and reduce energy loss. And it dissipates heat well, as well as it avoids the problems of unstable operation and small driving torque of the ultrasonic motor in the past. The polarization directions of the two groups of piezoelectric ceramic sheets are shown in Fig. 1.

2.2. Bending vibration of cylindrical shells

The piezoelectric oscillator described in this paper is a thin-walled structure, and its vibration modes can be analyzed by using the cylindrical shell vibration theory. The coordinate system of the cylindrical shell is shown in Fig. 2, which is the radial coordinate, the angular coordinate and the axial coordinate. It is assumed that the vibration displacement is tangential and radial. The displacement distribution of the in-plane vibration mode of the cylindrical shell is a constant along the axial direction (axis), and the displacement distribution along the radial direction (axis) is also considered as a constant due to the thin-walled structure, so each displacement component is a function of the angular coordinate. Soedel (2004) proposed the equation for the in-plane free vibration of a cylindrical shell:

$$\frac{\partial^2 x}{\partial\theta^2}+\frac{\delta y}{\delta\theta}+k\left(\frac{\partial^2 x}{\partial\theta^2}-\frac{\partial^3 y}{\partial\theta^3}\right)=-\frac{R^2}{K}\rho h\frac{\partial^2 x}{\partial t^2}, \quad (1)$$

$$\frac{\partial x}{\partial\theta}+y-k\left(\frac{\partial^3 x}{\partial\theta^3}-\frac{\partial^4 y}{\partial\theta^4}\right)=-\frac{R^2}{K}\rho h\frac{\partial^2 y}{\partial t^2}, \quad (2)$$

where $K=\frac{E}{(1-\mu^2)}$ is the short cylinder stiffness, $k=\frac{h^2}{12R^2}$ is the short cylinder correlation constant, h is the radial thickness, R is the neutral plane radius, ρ is the material density, μ is the material Poisson's ratio, E is the material Young's modulus.

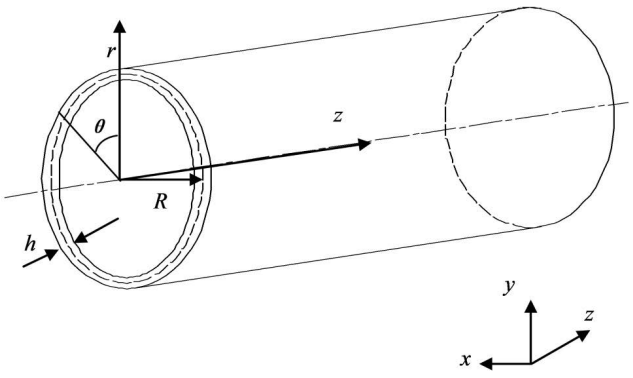

Fig. 2. Coordinates of cylindrical shells.

According to the periodicity of the ring structure, there are solutions of the following form:

$$\begin{pmatrix}x_{n1}\\ y_{n1}\end{pmatrix}=A_{n1}\begin{pmatrix}\sin n\theta\\ B_n\cos n\theta\end{pmatrix}\cos\omega t, \quad (3)$$

$$\begin{pmatrix}x_{n2}\\ y_{n2}\end{pmatrix}=A_{n2}\begin{pmatrix}\cos n\theta\\ -B_n\sin n\theta\end{pmatrix}\cos\omega t, \quad (4)$$

where ω is the circular frequency of the short cylinder, A_{n1}, A_{n2}, B_n are the amplitude coefficients. The aforementioned formula is substituted into the vibration equation to obtain:

$$\begin{vmatrix}\frac{K}{\rho hR^2}(1+k)n^2-\omega_n^2 & \frac{K}{\rho hR^2}n(1+kn^2)\\ \frac{K}{\rho hR^2}n(1+kn^2) & \frac{K}{\rho hR^2}(1+kn^4)-\omega_n^2\end{vmatrix}=0. \quad (5)$$

Solving Eq. (5) yields:

$$\omega_{n1}^2=\frac{1}{2}\frac{K}{\rho hR^2}[(1+k)n^2+kn^4+\sqrt{a^*}], \quad (6)$$

$$\omega_{n2}^2=\frac{1}{4}\left(\frac{K}{\rho hR^2}\right)^2[(1+k)n^2+kn^4-\sqrt{a^*}], \quad (7)$$

where

$$a^*=[(1+k)n^2+kn^4]^2+4n^2(1+kn^2)^2-4n^2(1+k)(1+kn^4).$$

Combining Eqs. (3) and (4) yields:

$$B_{n1}=\frac{\rho h\omega_{n1}^2R^2-n^2K(1+k)}{Kn(1+n^2k)}, \quad (8)$$

$$B_{n2}=\frac{\rho h\omega_{n2}^2R^2-n^2K(1+k)}{Kn(1+n^2k)}, \quad (9)$$

where ω_{n1} is the intrinsic frequency of the n-th-order in-plane expansion mode, ω_{n2} is the intrinsic frequency of the n-th-order in-plane bending mode. B_{n1}, B_{n2} are the in-plane bending modes of the short cylinder.

2.3. Principle of operation

Figure 3 shows the working principle of the inner cone ultrasonic motor proposed in this paper. The internal cone type vibrator structure has a certain symmetry. When the two-phase piezoelectric ceramic sheets arranged at 90° intervals are excited by the sine and cosine excitation voltages, respectively, the vibrator will generate a third-order bending resonance, and the vibrator will be excited:

$$w_A=W\cos n\theta\cos\omega t, \quad (10)$$

$$w_B=W\sin n\theta\sin\omega t. \quad (11)$$

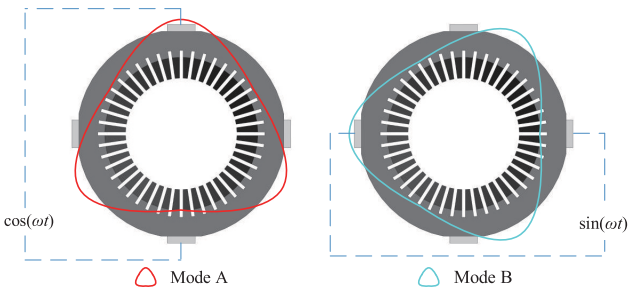

Fig. 3. Working principle of internal cone type ultrasonic motor.

A and B two-phase standing waves are superimposed on the vibrator to obtain bending traveling waves:

$$w = w_A + w_B = W\cos(n\theta - \omega t), \tag{12}$$

where W is the amplitude of the vibration of the A and B phases, n is the modal order of the bending vibration, θ is the angular coordinate along the circumferential direction, ω is the natural frequency of the third-order bending mode.

For the third-order bending mode, the two-phase ceramic sheets are separated by three-quarter wavelengths in this paper. When the two standing waves with equal amplitudes excited by the two modes A and B have a phase difference of $\pi/2$ in time, they will be superimposed on the internal cone type vibrator to form a traveling wave running in the circumferential direction. After the traveling wave is formed on the internal cone type vibrator, the two orthogonal in-plane third-order bending modes of the same frequency are superimposed on each other to generate an elliptical motion trajectory on the particle on the inner tooth surface. Finally, under the action of a certain pre-pressure, the rotary motion of the tapered rotor is realized through the friction coupling between the inner teeth and the tapered rotor.

3. Finite element simulation of piezoelectric vibrator

In this paper, modal and harmonic response analyses were performed with the help of the ANSYS finite element software to design and build an internal cone type vibrator model. Figure 4 shows the two third-order bending vibration patterns of the designed tapered vibrator under free boundary conditions.

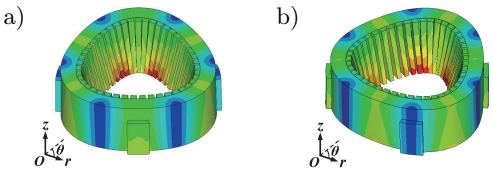

Fig. 4. Third-order bending mode of piezoelectric vibrator: a) B03 A-phase mode; b) B03 B-phase mode.

In selecting the vibrator vibration mode, the modal analysis results show that the vibrator is not only orthogonal but also similar in frequency in the third-order bending resonance mode. At the same time, the amplitude of the low-order mode is larger than that of the high-order mode in terms of vibration strength, so the low-order mode is usually chosen. Finally, the two orthogonal third-order bending modes of the piezoelectric vibrator are selected to have intrinsic frequencies of f_A = 22959.7 Hz and f_B = 22960.8 Hz.

In order to ensure that the vibrator does not have interference modes in a certain wide working frequency band, the ANSYS finite element software is used to analyze the harmonic response of the ultrasonic motor vibrator. An excitation signal with a peak value of 40 V and the frequency range of 20000 Hz to 25000 Hz was applied to the two sets of ceramic sheets, respectively. The amplitude-frequency characteristics of the vibrator are obtained through the analysis and solution of the post-processing module of the ANSYS finite element software. The amplitude displacement peak appeared at the frequency of 22960 Hz, and no other amplitude displacement peaks appeared in the frequency range 20000~25000 Hz. The results show that the vibrator has no interference mode in the frequency range, which verifies that the motor has good stability in a wide frequency band. The analysis results of the A and B phases are shown in Fig. 5.

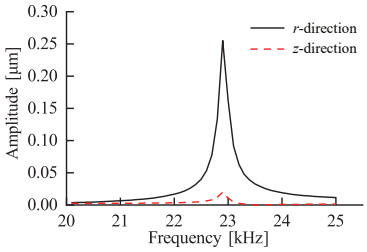

Fig. 5. Harmonic response analysis of vibrator.

4. Experimental study of ultrasonic motor

4.1. Prototype ultrasonic motor

The prototype of the cone type ultrasonic motor was made according to the structural dimensions given in Fig. 1. The vibrator material is 45# steel (high quality carbon structural steel with a carbon content of 0.45%), and the motor vibrator is boiled black in order to prevent the vibrator from being corroded by long working hours. Under certain pre-pressure, four rectangular PZT-81 piezoelectric ceramic sheets polarized along the thickness direction were attached to the four positioning slots on the outer cylindrical surface of the vibrator using epoxy resin. The length of PZT-81 piezoelectric ceramic sheet is 8 mm, the width is 4 mm, and the thickness is 1 mm. The detailed parameters are shown in Table 1. The bottom edge

Table 1. Properties of the piezoelectric ceramic sheet.

Ceramic	Piezoelectric strain factor d_{33} [pC·N^{-1}]	Relative permittivity ε_r	Planar electromechanical coupling coefficient k_p [%]	Thickness electromechanical coupling coefficient k_t [%]	Mechanical quality factor Q_m
PZT-81	300	1350	0.58	0.50	1000

of the rectangular piezoelectric ceramic sheet is aligned with the end of the small aperture of the vibrator. In order to reduce the wear on the vibrator during the long working hours of the motor, the tapered rotor material is 2A12 (series 2 aluminum alloy with serial number 12) with a weight of 10 g. The prototype is shown in Fig. 6.

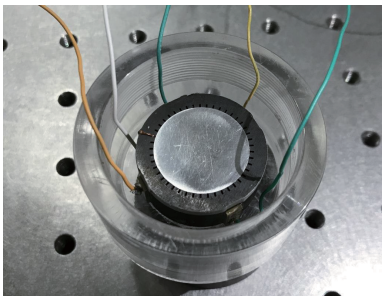

Fig. 6. Photograph of internal cone type ultrasonic motor principle prototype.

4.2. Ultrasonic motor vibrator test experiment

The vibration characteristics of the internal cone type vibrator were tested by the arbitrary waveform/function signal generator Tektronix AFG320, the 2713 Power Amplifier from B&K Denmark, the Germany Polytec OFV-505/5000 Laser Vibrometer, the multi-channel high frequency digital storage oscilloscope Agilent DS06014A and the precision vibration isolation platform as shown in Fig. 7. The frequency sweep test was carried out on the amplitude distribution of the midpoint P of the tooth structure end face of the inner tooth surface of the vibrator, as shown in Fig. 8.

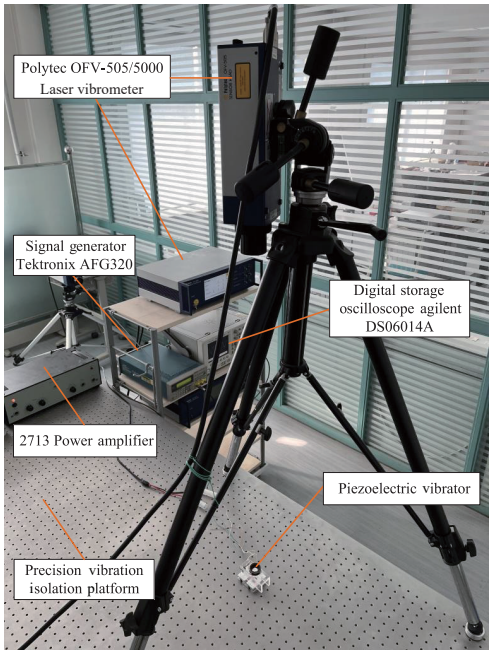

Fig. 7. Photograph of the experimental test instrument.

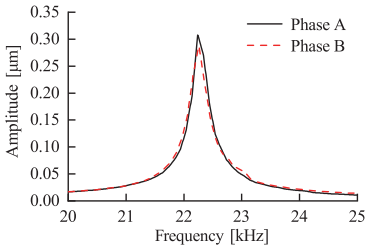

Fig. 8. Amplitude and frequency characteristics of the vibrator near the resonance point.

The experimental results show that the resonance frequencies of the two third-order bending modes of the vibrator are 22248.5 Hz and 22260 Hz, respectively, while the resonance frequencies obtained by modal analysis are 22959.7 Hz and 22960.8 Hz, respectively. The frequency difference between the two is 711.7 Hz and 700.8 Hz respectively, and the errors are 3.09% and 3.05%, respectively. The frequency of the third-order bending mode is basically consistent with the numerical simulation results of ANSYS software. The vibrator has no other interference modes in the frequency range of 20000~25000 Hz.

The amplitude distribution of the midpoint P of the tooth structure end face of the inner tooth surface of the vibrator was tested by a vibration testing instrument. The actual vibration measurement results are shown in Fig. 9. When the excitation frequency is 22260 Hz, the in-plane third-order bending mode of the vibrator can be well excited, and the vibrator can realize the expected traveling wave motion, which also proves the feasibility of the motor.

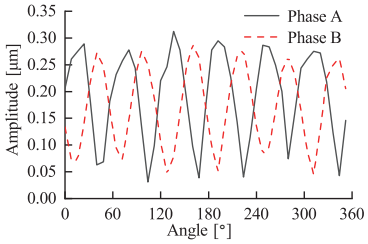

Fig. 9. 360° amplitude distribution of piezoelectric vibrator.

4.3. Ultrasonic motor vibrator test experiment

The output characteristics test rig was built (Fig. 10). The output characteristics of the motor are experimentally tested when the excitation voltage peak-to-peak value is 300 V and the excitation frequency is 22260 Hz using the multi-function driver. In the experimental test, a photoelectric tachometer was used to measure the rotational speed of the tapered rotor under different excitation voltages. When the excitation voltage peak-to-peak value is 300 V, the prepressure is 0.1 N, the excitation frequency is 22260 Hz, and the excitation voltage is increased to 300 V, the no-load speed of the ultrasonic motor can reach up to 441.2 rpm, as shown in Fig. 11.

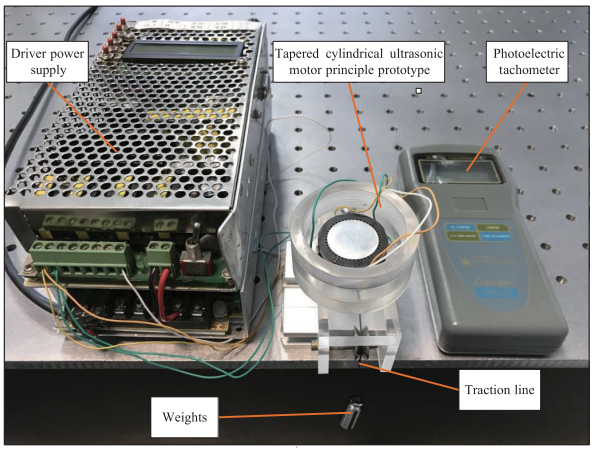

Fig. 10. Photograph of the output characteristics test rig.

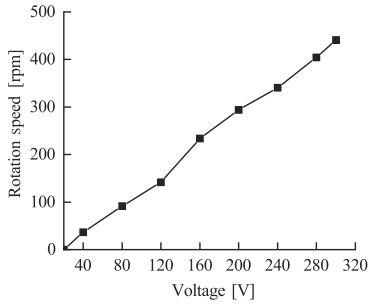

Fig. 11. No-load speed at different excitation voltages.

In the experimental test of torque and rotational speed, the magnitude of the torque is adjusted by lifting weights of different masses by the tapered rotor, while the rotational speed is still measured with a photoelectric tachometer. When the peak-to-peak value of the excitation voltage is 300 V, the pre-pressure is 0.1 N, and the excitation frequency is 22260 Hz, the motor speed decreases smoothly with the increase of torque, which is approximately linear. The maximum output torque of the motor is 1.06 N · mm, as shown in Fig. 12.

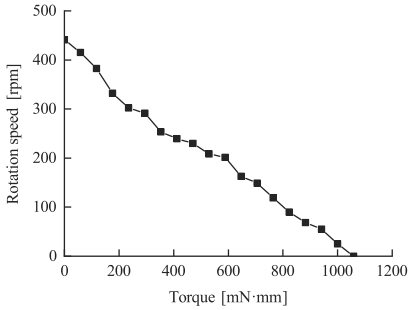

Fig. 12. Motor speed at different torques.

4.4. Ultrasonic motor pre-pressure analysis

The optimum ultrasonic motor pre-pressure depends on the design parameters and operating torque of the motor. When assembling a motor, choosing different pre-pressure for specific operating conditions and load torques will positively affect its efficiency and performance. The test was performed with the output characteristics test rig above (Fig. 10). The platform is capable of applying loads and pre-pressure forces and testing the corresponding speeds. In the experimental tests of pre-pressure, load torque and rotational speed, the pre-pressure was adjusted by changing the weight and load of the tapered rotor. The torque is regulated by tapered rotors that lift different masses, while speed is still measured by a photoelectric tachometer.

The motor speed decreases as the load torque increases until the motor is locked. On the other hand, the motor speed increases as the pre-pressure increases and then decreases, as shown in Fig. 13. As can be seen from the figure, the pre-pressure and load torque do not affect the motor speed independently; the coupling between pre-pressure and load torque is as follows: as the load torque increases, the value of the optimal motor pre-pressure corresponds to the inflection point of the speed increase.

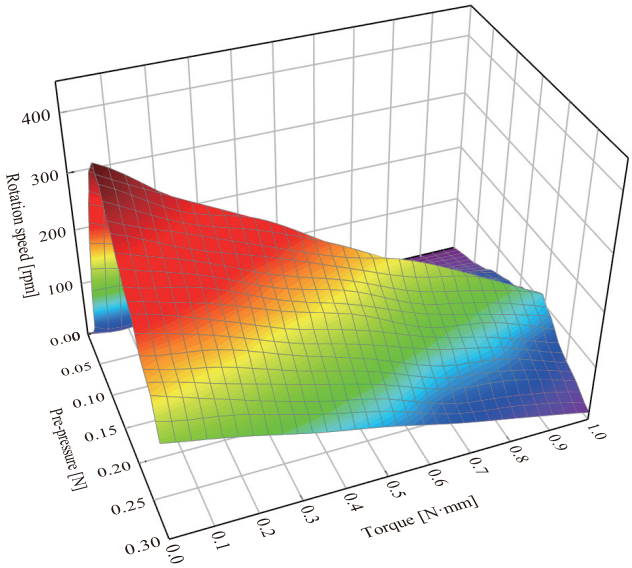

Fig. 13. Relationship between the experimentally found motor speed, pre-pressure, and load torque.

At present, the speed regulation methods of ultrasonic motors mainly include frequency regulation, voltage regulation, and phase regulation. The existing speed regulation methods often have the problem of coupling the speed and torque, as well as the narrow adjustment range. For such problems, we propose to change the pre-pressure speed regulation scheme and conduct a pre-pressure speed regulation experiment for this motor. According to the experimental results, the relationship between motor speed and pre-pressure under different loads can be obtained, as shown in Fig. 14.

As can be seen from Fig. 14, the motor speed increases and then decreases with increasing pre-pressure for all cases with different load torques. By using this monotonic relationship fragment before and after the

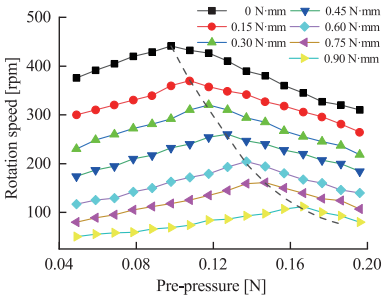

Fig. 14. Relationship between speed and pre-pressure under different loads.

pre-pressure reaches a specific value, the motor speed can be adjusted. In addition, for fast speed regulation and to avoid non-monotonic relationship in speed regulation, the pre-pressure should be gradually increased from the left side for small load torque and gradually decreased from the right side for large load torque until the motor reaches the desired speed. The dashed line marks the trend of the pre-pressure corresponding to the maximum speed of the motor at different load torques. It can also be seen that there is no sudden blocking of the motor when increasing the pre-pressure; theoretically a full range of speed regulation can be achieved.

5. Conclusion

With the help of the ANSYS finite element software, a parametric model of an internal cone type rotating traveling wave ultrasonic motor with trapezoidal teeth was established. The modal analysis and harmonic response analysis of the motor vibrator were carried out, and the structural parameters and working modes were determined. A prototype was fabricated, and the vibration characteristics of the motor vibrator were tested by the laser vibration measurement system, and the excitation frequency of the two orthogonal modes with the same frequency was 22260 Hz. An output performance test device was built, and the output characteristics of the prototype were tested experimentally. The prototype runs stably, has a high-speed output, and has good motion and power adjustment characteristics. When the excitation voltage peak-to-peak value is 300 V, the pre-pressure is 0.1 N, and the excitation frequency is 22260 Hz, the maximum output torque of the ultrasonic motor is 1.06 N · mm, and the maximum no-load speed is 441.2 rpm. The optimal pre-pressure of the motor under different loads is studied and analyzed. There is a coupling relationship between the influence of pre-pressure and load torque on the speed of the ultrasonic motor. Adjusting the pre-pressure according to the load and rotational speed can improve the output efficiency of the ultrasonic motor. This has important implications for the practical use of this ultrasonic motor.

Acknowledgments

This research was funded by the Natural Science Foundation of Liaoning Provincial Department of Science and Technology (grant no. 2022-BS-307) and the Basic Research Project of Education Department of Liaoning Province (grant no. JJL202015401).

References

1. Čeponis A., Mažeika D., Vasiljev P. (2020), Flat cross-shaped piezoelectric rotary motor, *Applied Sciences*, **10**(14): 5022, doi: 10.3390/app10145022.
2. Li H., Deng J., Zhang S., Yu H., Liu Y. (2021), Design and experiment of a three-feet linear ultrasonic motor using third bending hybrid modes, *Sensors and Actuators A: Physical*, **331**: 112990, doi: 10.1016/j.sna.2021.112990.
3. Li S. *et al.* (2019), Tailoring friction interface with surface texture for high-performance ultrasonic motor friction materials, *Tribology International*, **136**: 412–420, doi: 10.1016/j.triboint.2019.03.072.
4. Liu R. *et al.* (2022), A precision positioning rotary stage driven by multilayer piezoelectric stacks, *Precision Engineering*, **76**: 226–236, doi: 10.1016/j.precisioneng.2022.03.013.
5. Lu D., Lin Q., Chen B., Jiang C., Hu X. (2020), A single-modal linear ultrasonic motor based on multi vibration modes of PZT ceramics, *Ultrasonics*, **107**: 106158, doi: 10.1016/j.ultras.2020.106158.
6. Makarem S., Delibas B., Koc B. (2021), Data-driven tuning of PID controlled piezoelectric ultrasonic motor, *Actuators*, **10**(7): 148, doi: 10.3390/act10070148.
7. Mashimo T., Oba Y. (2022), Performance improvement of micro-ultrasonic motors using the thickness shear mode piezoelectric elements, *Sensors and Actuators A: Physical*, **335**: 113347, doi: 10.1016/j.sna.2021.113347.
8. Mishra J.P., Xu Q., Yu X., Jalili M. (2018), Precision position tracking for piezoelectric-driven motion system using continuous third-order sliding mode control, [in:] *IEEE/ASME Transactions on Mechatronics*, **23**(4): 1521–1531, doi: 10.1109/TMECH.2018.2853737.
9. Oh J.-H. *et al.* (2009), Design and performances of high torque ultrasonic motor for application of automobile, *Journal of Electroceramics*, **22**(1): 150–155, doi: 10.1007/s10832-008-9434-1.
10. Olsson P., Nysjö F., Carlbom I.B., Johansson S. (2016), Comparison of walking and traveling-wave piezoelectric motors as actuators in kinesthetic haptic devices, [in:] *IEEE Transactions on Haptics*, **9**(3): 427–431, doi: 10.1109/TOH.2016.2537803.
11. Puoza J.C., Sakthivelsamy R. (2021), Ultrasonic motors structural design and tribological performance – A review, *Tribology Online*, **16**(4): 286–298, doi: 10.2474/trol.16.286.

12. Ryndzionek R., Sienkiewicz Ł. (2021), A review of recent advances in the single- and multi-degree-of-freedom ultrasonic piezoelectric motors, *Ultrasonics*, **116**: 106471, doi: 10.1016/j.ultras.2021.106471.
13. Soedel W. (2004), *Vibrations of Shells and Plates*, CRC Press, USA.
14. Tian X., Liu Y., Deng J., Wang L., Chen W. (2020), A review on piezoelectric ultrasonic motors for the past decade: Classification, operating principle, performance, and future work perspectives, *Sensors and Actuators A: Physica*, **306**: 111971, doi: 10.1016/j.sna.2020.111971.
15. Wang H., Pan Z., Zhu H., Guo Y. (2020), Pre-pressure influences on the traveling wave ultrasonic motor performance: A theoretical analysis with experimental verification, *AIP Advances*, **10**(11): 115211, doi: 10.1063/5.0028282.
16. Wang P., Xu Q. (2017), Design and testing of a flexure-based constant-force stage for biological cell micromanipulation, [in:] *IEEE Transactions on Automation Science and Engineering*, **15**(3): 1114–1126, doi: 10.1109/TASE.2017.2733553.
17. Xu D., Yang W., Zhang X., Yu S. (2021), Design and performance evaluation of a single-phase driven ultrasonic motor using bending-bending vibrations, *Micromachines*, **12**(8): 853, doi: 10.3390/mi12080853.
18. Zhang P., Niu J., Zhang X., Mao S., Liu J., Yang B. (2022), Thick film ultrasonic micromotor based on chemical mechanical thinning and polishing process, [in:] *IEEE Electron Device Letters*, **43**(9): 1547–1550, doi: 10.1109/LED.2022.3195349.
19. Zhao C. (2011), *Ultrasonic Motors: Technologies and Applications*, Springer, China.
20. Zhao Y., Yuan S., Chu X., Gao S., Zhong Z., Zhu C. (2016), Ultrasonic micro-motor with multilayer piezoelectric ceramic and chamfered driving tips, *Review of Scientific Instruments*, **87**(9): 095108, doi: 10.1063/1.4963662.